NEW TECHNIQUES FOR OPERATION AND DIAGNOSTICS OF RELATIVISTIC ELECTRON COOLERS

M. W. Bruker, A. Hofmann, E. Riehn, T. Weilbach, K. Aulenbacher, J. Dietrich
Helmholtz Institute Mainz, Germany

W. Klag
Institute for Nuclear Physics Mainz, Germany

M. I. Bryzgunov, V. Parkhomchuk, V. B. Reva
BINP SB RAS, Novosibirsk, Russia

Abstract

The Helmholtz Institute Mainz (HIM) performs experiments related to possible improvements of high-energy d.c. electron coolers. Results and activities concerning non-invasive beam diagnostics and beam control at large operating currents will be shown. Furthermore, progress of our project to use turbo generators as a means for potential-free power generation in high-energy electron coolers is presented.

INTRODUCTION

High-intensity electron beams are getting more and more popular (e.g. in planned electron cooling devices) but make high demands on diagnostics and power supplies. With an energy of several MeV and a current of amperes, the use of conventional destructive diagnostic tools is very limited just as the use of conventional power supplies is. In this paper we present three experimental set-ups connected to high-energy electron coolers: non-invasive beam diagnostics, the impact of secondary electron emission in energy recovery machines and turbine-driven power supplies for focusing magnets. All experiments have been performed at the Institute of Nuclear Physics and the Helmholtz Institute in Mainz.

EXPERIMENTAL SET-UP FOR MEASUREMENT OF SECONDARY CURRENT

The energy recovery method used in electron coolers results in secondary electrons emitted from the collector surface being re-accelerated, possibly harming operational stability. Research done by BINP indicates that a Wien filter as part of the collector optics is a suitable means to suppress electron backflow, increasing the total recuperation efficiency by a factor of 100 [1]. However, stopping these particles in turn creates new secondaries with a different energy and angle distribution. This gives rise to a cascade that depends heavily on the geometry of the electrodes and the vacuum chamber.

HIM operates a test set-up capable of providing a magnetized 17 keV, 0.5 A electron beam and measuring the currents flowing onto the relevant aperture plates independently. A sketch of the device including the distribution of electric potentials is shown in Fig. 1.

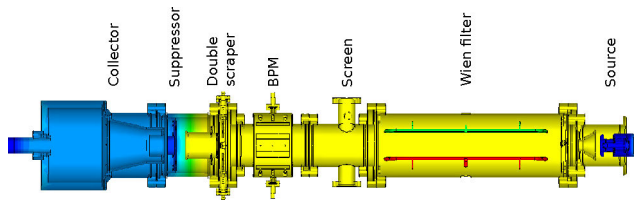

Figure 1: Schematic view of the vacuum chamber. Blue: $U < 0$. Yellow: $U = 0$.

The potential minimum inside the suppressor electrode results in secondary electrons with an energy $E_{\mathrm{kin}} < e\left|U_{\mathrm{col}} - U_{\mathrm{sup}}\right|$ being reflected to the collector. By varying this potential, secondary losses can be distinguished from primary losses. In the absence of primary losses, the integrated energy spectrum of secondary electrons exiting the collector can be obtained except for the elastic peak. Figure 2 shows that while the shape of the spectrum is what can be expected [2], several surfaces contribute to the total losses because of higher generations of secondary electrons emitted from the deceleration aperture plate and the Wien filter collector plate.

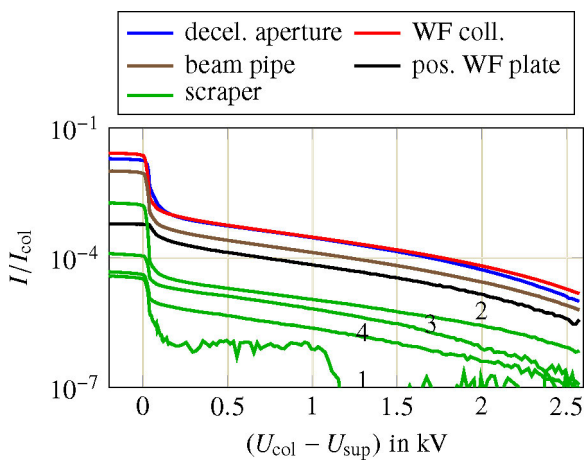

Figure 2: Secondary currents vs. suppressor voltage. $I_{\mathrm{col}} = 20\,\mathrm{mA}$.

These losses are irrelevant to the cooler as long as the particles cannot enter the high-energy section. To determine the possible trajectories of higher-generation secondary elec-

ISBN 978-3-95450-181-6

trons that can cause a non-zero current out of the Wien filter given a suitable aperture, detailed computer simulations were performed. These show that the total secondary current exiting the collector optics can be estimated to be of the order of $10^{-9}\, I_{\mathrm{col}}$, rendering the problem negligible in comparison with other unwanted effects such as residual gas ionization. More details can be found in [3].

TURBINE-DRIVEN POWERING OF HV COMPONENTS

One of the challenges in the development of a relativistic electron cooler is the powering of components, e.g. HV solenoids, which sit on different high potentials within a high voltage vessel and therefore need a floating power supply. A modular power supply with two cascade transformers per module would overcome the many disadvantages of a conventional setup. Either the transformers that power the HV solenoids or the solenoids themselves are then fed by a turbo generator powered by pressurized gas. A promising candidate for the needed turbo generator could be the Green Energy Turbine (GET) designed by company DEPRAG, which works with dry air and delivers a power of 5 kW. At the Helmholtz Institute Mainz (HIM) two of these generators have been tested for performance and durability. Figure 3 gives an overview of the experimental setup.

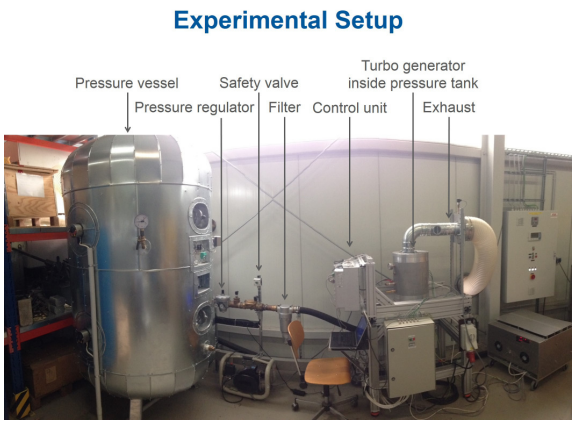

Figure 3: First set-up of the GET test facility at HIM. The main components are (from left to right): a pressure vessel, pressure regulators and safety valves, a control unit, the turbo generator itself and the exhaust.

Since the turbo generator will be placed inside an SF_6 vessel later, all experiments have been performed with the GET inside a pressurized tank with 10 bar. The relation between the inlet pressure (or the revolution speed, respectively) and the delivered DC power can be found in Fig. 4.

NON-DESTRUCTIVE DIAGNOSTIC METHODS

Two different methods to measure the beam profile will be presented in the following section, namely Thomson Laser Scattering (TLS) and Beam-Induced Fluorescence (BIF).

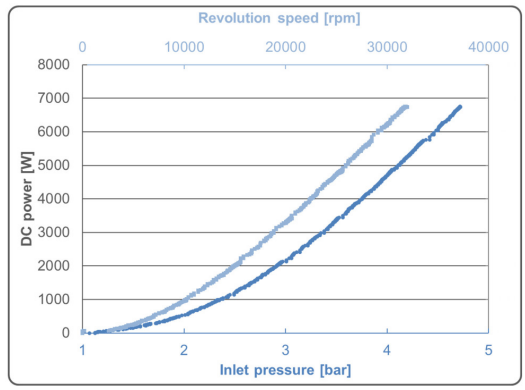

Figure 4: DC power versus revolution speed / inlet pressure of the green energy turbo generator.

Thomson scattering describes elastic scattering of a photon off a free electron and is basically the low-energy limit of the Compton scattering process. A photon λ_{L} hits the electron beam at an angle Θ and is scattered with the scattering angle Θ'. Due to the Doppler shift the scattered photon λ_{S} gains energy. The wavelength of the scattered photon as a function of the angle between the incident photon and electron and the angle between scattered photon and electron can be evaluated by

$$\lambda_{\mathrm{S}} = \lambda_{\mathrm{L}} \frac{(1 + \beta \cos \Theta')}{(1 + \beta \cos \Theta)} \tag{1}$$

where β is the electron velocity in units of the speed of light. The number of scattered photons can be calculated by using the following equation:

$$R = \frac{1}{2} r_e^2 \left(1 + \cos^2 \Theta'\right) N_L n_e P \epsilon \Delta\Omega l \frac{(1 + \beta \cos(\Theta))}{(1 + \beta \cos(\Theta'))\gamma} \tag{2}$$

with r_e = classical electron radius, N_L = number of incident photons per Joule, n_e = electron density, P = laser power, ϵ = detector system efficiency, $\Delta\Omega$ = detector solid angle, l = interaction length, $\frac{(1+\beta\cos(\Theta))}{(1+\beta\cos(\Theta'))\gamma}$ = factor resulting from Lorentz transformation.

In our experiment we set Θ to be 90° and Θ' to be 135°. With an electron energy of 100 keV, a current of 25 mA, P = 130 W, ϵ = 0.17, $\Delta\Omega$ = 0.01, l = 3 mm (beam diameter), the count rate is expected to be 5 Hz. Because of the low count rate, reducing or at least controlling the background is crucial. By carefully adjusting the beam optics, blackening the beam pipes and using a coincidence unit, the background has been reduced from 200 Hz to below 10 Hz, making TLS profile measurements possible in the first place.

Figure 5 shows a half section of the CAD model of the TLS chamber. The paths of the electron beam, the incident Laser beam, and the scattered photons are indicated. Due to the limited space, the detector cannot be placed in the scattering plane. Therefore, an imaging system consisting of a lens and a parabolic mirror images the interaction region onto the PMT passing two bandpass filters that reduce the background created by the laser.

ISBN 978-3-95450-181-6

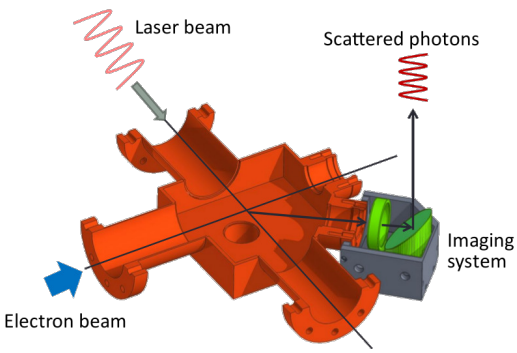

Figure 5: Half section of the TLS chamber (orange) and the detector system. The angle between laser and electron beam is $\Theta = 90°$ whereas $\Theta' = 135°$ is the angle between electron beam and scattered photons. The imaging system (green) consists of a lens and a parabolic mirror.

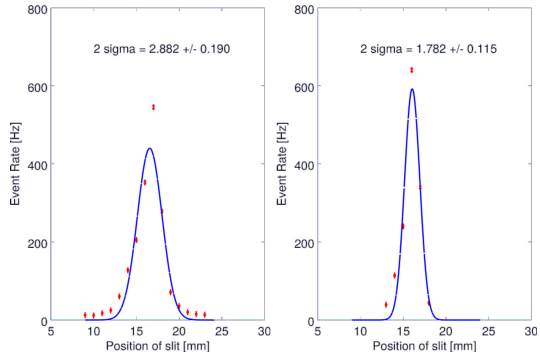

Figure 6: BIF measurement with statistical errors for different focusing strengths of the solenoid in front of the BIF chamber. The measurement is shown in red and the Gaussian fit in blue. Left: Solenoid current 50 mA, right: Solenoid current 500 mA.

The rate of the scattered photons is proportional to the integrated electron density along the path of the laser through the electron beam. By moving the laser beam through the electron beam vertically, a profile measurement can be done. Due to the low cross section, which is mostly dominated by the classical electron radius squared, the required laser power is very high (150 W). The electron beam to be measured is generated by illuminating a photocathode with a second laser system. In order to achieve the required peak current of about 30 mA, the latter has to be pulsed, making it necessary to synchronize both laser systems.

For protons and ions, beam profile measurement based on beam-induced fluorescence is a common technique [4]. The idea is to image the fluorescing residual gas on a photo detector with a spatial resolution. Instead of a detector with a spatial resolution, a photomultiplier tube (PMT) with a movable slit in front of it can be used.

The intensity of the photons is proportional to the pressure and the beam current. A gas dosing valve is used to insert N_2 gas into the vacuum system, which then converts 3.6 keV of average energy loss into one visible photon [5]. Since N_2 can be pumped out of the vacuum system very easily, residual gas pressures of 10^{-5} mbar can be generated in the BIF chamber without impacting other parts of the apparatus.

Figure 6 shows typical experimental results from a measurement with a beam current of 75 µA and two different settings of a focusing solenoid. It can clearly be seen that the width of the beam changes with respect to the focusing strength of the solenoids. A Gaussian function (blue) is fitted to the measured values including statistical errors (red) to extract the beam width.

CONCLUSIONS

Simulations of secondary electron trajectories using CST have been performed and are in very good agreement with experimental data. It could be shown that using a Wien filter and suitable collector optics, secondary emission from the collector surface poses no concern to the operation of future electron coolers. The turbo generator GET has been shown to deliver the sufficient power of 5 kW over a period of more than 1000 h without maintenance. An even further improvement regarding the lifetime would be a turbine with air bearings, which is under development at the moment. The laser system and the electron gun for both the TLS and the BIF measurements have been installed. With a signal-to-noise ratio of 50 %, the measurement still seems challenging but possible.

REFERENCES

[1] M. Bryzgunov et al., "Efficiency Improvement of an Electron Collector Intended for Electron Cooling Systems Using a Wien Filter", Technical Physics Vol. 58 No. 6, 2013.

[2] H. Bruining, "Physics and applications of secondary electron emission", 1954.

[3] M. Bruker, "Untersuchung der Rückgewinnungseffizienz eines Kühlerelektronenstrahls in longitudinalem Magnetfeld" (in German), PhD thesis, University of Mainz, Germany, 2016.

[4] F. Becker, "Beam Induced Fluorescence Monitors", WEODO1, Proceedings of DIPAC 2011, Hamburg, Germany.

[5] M.A. Plum et al., Nucl. Instr. Meth. A 492 (2002), p. 74.

ISBN 978-3-95450-181-6